

# Architecture of the RNA Polymerase II-TFIIS Complex and Implications for mRNA Cleavage

Hubert Kettenberger, Karim-Jean Armache,  
and Patrick Cramer\*

Institute of Biochemistry  
Gene Center  
University of Munich  
Feodor-Lynen-Str. 25  
81377 Munich  
Germany

## Summary

The transcription elongation factor TFIIS induces mRNA cleavage by enhancing the intrinsic nuclease activity of RNA polymerase (Pol) II. We have diffused TFIIS into Pol II crystals and derived a model of the Pol II-TFIIS complex from X-ray diffraction data to 3.8 Å resolution. TFIIS extends from the polymerase surface via a pore to the internal active site, spanning a distance of 100 Å. Two essential and invariant acidic residues in a TFIIS loop complement the Pol II active site and could position a metal ion and a water molecule for hydrolytic RNA cleavage. TFIIS also induces extensive structural changes in Pol II that would realign nucleic acids in the active center. Our results support the idea that Pol II contains a single tunable active site for RNA polymerization and cleavage, in contrast to DNA polymerases with two separate active sites for DNA polymerization and cleavage.

## Introduction

Synthesis of eukaryotic mRNA from protein-coding genes is carried out by RNA polymerase (Pol) II. The mechanism of mRNA transcription has recently been elucidated with crystallographic structures of yeast Pol II in various forms (reviewed in Cramer, 2002a; Woychik and Hampsey, 2002). These structures include the ten-polyptide core of Pol II in free form (Cramer et al., 2000, 2001), in form of an elongation complex with DNA and RNA (Gnatt et al., 2001), and in complex with the toxin  $\alpha$ -amanitin (Bushnell et al., 2002). Backbone models of the complete 12-subunit Pol II, including the core and the two additional subunits Rpb4 and Rpb7, have just been reported (Armache et al., 2003; Bushnell and Kornberg, 2003).

In the structures, the two large Pol II subunits, Rpb1 and Rpb2, line an active center cleft. One side of the cleft is formed by a mobile “clamp,” which is connected to the remainder of Pol II by five protein “switch” regions. During elongation, DNA enters the cleft at two “jaws,” the Rpb1/9 jaw and the Rpb5 jaw, and is unwound before the active center. The DNA template strand binds to switch regions 1 and 2, and to the “bridge” helix, which spans the cleft. Beyond the bridge, the DNA template strand and the nascent RNA form a nine base pair DNA-RNA hybrid, which is bent by nearly 90° with respect to

incoming DNA. The bridge lines a “pore” beneath the active site, which widens toward the “bottom” face of Pol II, creating an inverted “funnel.” The active site comprises a metal ion, called metal A, which is bound by the Rpb1 “aspartate loop” at the entrance to the pore. Another metal ion can bind weakly further in the pore (Cramer et al., 2001). The relative location of nucleic acids with respect to the two metal sites suggested that RNA polymerization could involve a two-metal-ion mechanism similar to that of DNA polymerases (reviewed in Cramer, 2002b).

Elongation of the mRNA chain is generally processive, due to tight binding of a stable DNA-RNA hybrid by Pol II. However, elongation can be blocked in various ways (reviewed in Erie, 2002; Shilatifard et al., 2003). Certain DNA sequences destabilize the DNA-RNA hybrid, causing reverse movement of Pol II (Nudler et al., 1997). Such “backtracking” involves detachment of the RNA 3' end from DNA and apparently RNA extrusion into the pore (Cramer et al., 2000). Backtracking by a few nucleotides results in pausing, a temporary block to elongation, from which Pol II can escape by itself. More extensive backtracking however can lead to transcriptional arrest. Escape from arrest requires cleavage of the extruded RNA with the help of the elongation factor TFIIS (reviewed in Fish and Kane, 2002; Wind and Reines, 2000).

TFIIS strongly enhances a weak RNA nuclease activity that is intrinsic to Pol II (Reines, 1992; Izban and Luse, 1992; Wang and Hawley, 1993). The nuclease activity represents the second enzymatic function of the enzyme beside RNA polymerization (and its reverse reaction, pyrophosphorolysis). Addition of TFIIS to paused and arrested elongation complexes releases RNA dinucleotides and 7–9-mers, respectively (Gu and Reines, 1995). In vitro, TFIIS-induced RNA cleavage can promote proofreading by Pol II, which enhances the fidelity of transcription by a mechanism subsequent to nucleotide incorporation (Thomas et al., 1998). TFIIS was the first Pol II transcription factor to be purified, based on promotion of efficient synthesis of long RNAs in vitro (Sekimizu et al., 1976). In keeping with the general functions of TFIIS in mRNA transcription, chromatin immunoprecipitation assays showed that TFIIS can associate with transcribing Pol II in vivo (Pokholok et al., 2002).

TFIIS is a modular factor that comprises an N-terminal domain I, a central domain II, and a C-terminal domain III. The weakly conserved domain I forms a four-helix bundle (Booth et al., 2000) and is not required for TFIIS activity. Domain II forms a three-helix bundle (Morin et al., 1996; Olmsted et al., 1998), and domain III adopts a zinc-ribbon fold with a thin protruding  $\beta$ -hairpin (Olmsted et al., 1998; Qian et al., 1993). Domain II and the linker between domains II and III are required for Pol II binding, whereas domain III is essential for stimulation of RNA cleavage.

To investigate the molecular mechanism of TFIIS-stimulated RNA cleavage, we have determined a detailed three-dimensional model for the Pol II-TFIIS multiprotein complex from X-ray crystallographic data extending to 3.8 Å resolution. The Pol II-TFIIS complex model shows the

\*Correspondence: cramer@LMB.uni-muenchen.de

Table 1. X-Ray Structural Analysis of the RNA Polymerase II-TFIIS Complex

Crystal	Native	TFIIS SeMet
Data collection <sup>a</sup>		
Unit cell dimensions (Å) <sup>b</sup>	218.9 × 395.3 × 281.0	219.7 × 394.9 × 282.3
Wavelength (Å)	0.9790	0.9795
Resolution range (Å) <sup>c</sup>	50–3.8 (3.94–3.8)	50–6.5 (6.73–6.5)
Unique reflections <sup>c</sup>	115 508 (9618)	24 571 (2407)
Completeness (%) <sup>c</sup>	96.2 (81.0)	100 (100)
Redundancy <sup>c</sup>	2.9 (1.2)	6.1 (6.1)
Mosaicity (°)	0.21–0.53 <sup>d</sup>	0.40
R <sub>sym</sub> (%) <sup>c</sup>	8.9 (35.5)	7.1 (32.6)
I/σ(I) <sup>3</sup>	9.3 (1.9)	11.6 (4.6)
Peaks in anomalous Fourier	8 Zn in Pol II (10.9–5.1σ) 1 Zn in TFIIS (9.1σ)	8 Zn in Pol II (11.6–7.4σ) 1 Zn in TFIIS (4.5σ) 1 Se in TFIIS (7.3σ)

<sup>a</sup> Diffraction data were collected at beamline X06SA at the Swiss Light Source.

<sup>b</sup> Crystals belong to the space group C222.

<sup>c</sup> Values in parentheses correspond to the highest resolution shell.

<sup>d</sup> Due to radiation damage, the mosaicity increased during data collection, and was refined in segments of 10°.

relative location of the interacting proteins. Comparison with previous Pol II structures reveals TFIIS-induced structural changes in Pol II, and the relative location of TFIIS with respect to nucleic acids, suggesting the mechanisms of TFIIS-regulated Pol II transcription.

## Results and Discussion

### Structural Analysis

The 12-subunit yeast Pol II was prepared as described (Armache et al., 2003) and crystallized under altered conditions (compare Experimental Procedures). Harvested crystals were incubated with a recombinant, fully active TFIIS variant that comprises domains II and III. The very large solvent channels of the crystals allowed TFIIS entry and binding to its specific site on Pol II, which is not obstructed by crystal contacts. It is intriguing that the crystal lattice can accommodate extensive structural changes induced by TFIIS (see below). The resulting 13-polypeptide asymmetric complex has a molecular weight of 536 kDa. The crystals have a large unit cell, a very high solvent content of almost 80%, and are highly radiation-sensitive. Diffraction data to 3.8 Å resolution could nevertheless be obtained with the use of cryocooling, synchrotron radiation, and a careful data collection strategy (Table 1).

Initial electron density maps were phased with the core Pol II structure and were improved by solvent flipping (compare Experimental Procedures). These maps showed positive difference density on the Pol II surface, which could to a large extent be accounted for with the rigid cores of the NMR structures of TFIIS domains II and III (Morin et al., 1996; Qian et al., 1993; Olmsted et al., 1998; Figures 1A and 2A). The positioning of the TFIIS domains was confirmed by locating a selenomethionine residue in domain II and the zinc ion in domain III with the use of anomalous signals (Figure 1B, Table 1). Also visible in the first electron density map were a long linker between the two TFIIS domains, and extensive structural changes in Pol II. Pol II regions that had shifted were omitted from electron density calculation and were manually docked to the resulting map. After rigid body refinement, the quality of the map was very high, and large protein side chains were generally visible. Newly

ordered Pol II regions were modeled as C $\alpha$ -backbones, as were TFIIS regions not accounted for by the NMR structures. The resulting model comprises all 12 Pol II subunits and the functional region of TFIIS (residues 148–309, Figure 2A).

### TFIIS Extends from a Polymerase Jaw to the Active Site

The model shows that TFIIS extends along the Pol II surface, spanning a distance of 100 Å (Figures 2 and 1B). Based on visual inspection of the model, we have redefined the domain borders of TFIIS (Figure 2A). To describe interactions of TFIIS with Pol II, we refer to the nomenclature of Pol II domains and secondary structure elements introduced previously (Cramer et al., 2001). TFIIS domain II docks to the exposed Rpb1 jaw domain of Pol II. The TFIIS interdomain linker extends from domain II along the Pol II surface into the funnel (Figure 2C). Domain III inserts into the Pol II pore, and approaches the polymerase active site from the bottom face of the enzyme as predicted (Cramer et al., 2000). The binding sites for domain III and  $\alpha$ -amanitin overlap, explaining why the toxin interferes with TFIIS activity (Izban and Luse, 1992; Rudd and Luse, 1996; Weillbaecher et al., 2003).

TFIIS domain II comprises a bundle of three helices ( $\alpha$ 1– $\alpha$ 3, Figure 2), which had been observed for the isolated domain by NMR (Morin et al., 1996), and three short helices, which form upon Pol II interaction ( $\alpha$ 4– $\alpha$ 6). TFIIS helices  $\alpha$ 1 and  $\alpha$ 3 pack against helix  $\alpha$ 40 in the Rpb1 jaw, to bury leucines L1172 and L1176 in helix  $\alpha$ 40 (Figure 3A). An acidic loop following Rpb1 helix  $\alpha$ 40 interacts with a basic patch on TFIIS helix  $\alpha$ 3, which includes residues required for TFIIS-Pol II interaction (Figure 3A; Awrey et al., 1998). In addition, TFIIS helix  $\alpha$ 6 contacts Rpb1 loop  $\beta$ 30– $\beta$ 31 (Figure 3A). Consistently, mutation of residue E1230 in this loop weakens Pol II binding to TFIIS (Wu et al., 1996). The location of TFIIS domain II at the Rpb1/9 jaw, next to the point of DNA entry to the cleft, may be relevant for interaction of TFIIS with the chromatin remodeling complex Swi/Snf, revealed in a genetic screen (Davie and Kane, 2000).

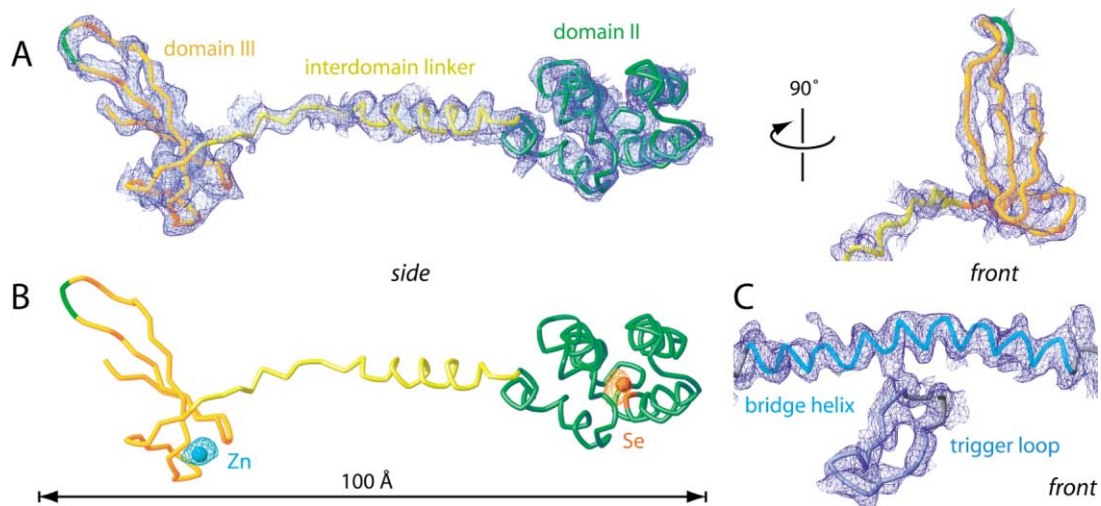


Figure 1. Structural Analysis of the Pol II-TFIIS Complex

(A) Electron density omit map. The map is contoured at  $1.0 \sigma$  and was calculated after solvent flipping using phases from the positioned atomic model of the 10-subunit Pol II. Omitted from map calculation were the TFIIS model, the Rpb4/7 complex, the bridge helix, and newly ordered elements of Pol II such as the trigger loop. TFIIS is depicted as a ribbon model. TFIIS domain II, the interdomain linker, and domain III are colored in green, yellow, and orange, respectively, and this color code is used throughout. The light green ribbon fragment in domain III corresponds to the acidic hairpin residues D290 and E291. The side view is as in Gnatt et al. (2001), and the front view is as in Armache et al. (2003) and Cramer et al. (2000, 2001).

(B) Anomalous difference Fourier maps. The Fouriers were calculated from anomalous differences in native (cyan net) and TFIIS-SeMet (orange net) data, and were contoured at  $2.5 \sigma$  and  $3.0 \sigma$ , respectively. Peaks in the anomalous Fouriers coincide with the position of a zinc ion in domain III (cyan sphere) and a selenium atom in M182 of domain II (orange sphere).

(C) Electron density omit map shown in (A). Depicted are the Pol II bridge helix and trigger loop, which were omitted from map calculation. Figures were prepared with RIBBONS (Carson, 1997).

### TFIIS Opens a Crevice in the Funnel

The TFIIS interdomain linker is unstructured in free TFIIS (Olmsted et al., 1998). Upon Pol II binding, however, the linker forms an  $\alpha$ -helix ( $\alpha 7$ ), which runs along the Pol II bottom face, near loop  $\beta 29$ - $\alpha 41$  and helix  $\alpha 38$  in Rpb1 (Figure 3A). At the end of helix  $\alpha 7$ , the linker passes through a narrow “crevice” into the funnel (Figure 2C). The crevice is lined by loop  $\alpha 20$ - $\alpha 21$  in the Rpb1 funnel domain on one side, and by strand  $\beta 32$  in the Rpb1 cleft domain on the other (Figure 3). The crevice is closed in previous Pol II structures, and opening of the crevice by TFIIS is partly responsible for major structural changes in Pol II (see below). The induced folding and polymerase interactions of the TFIIS linker are important for function. Linker residues contribute to TFIIS activity (Awrey et al., 1998), and confer species-specificity to the Pol II-TFIIS interaction (Shimasaki and Kane, 2000). Mutations that change the linker length abolish TFIIS activity, and isolated domains II and III are not functional (Awrey et al., 1998).

### TFIIS Domain III Inserts into the Pore

TFIIS domain III is bound with its zinc binding base at the entrance to the pore on the bottom face of Pol II (Figures 2B, 2C, and 3B). The thin  $\beta$ -hairpin of domain III extends along one side of the pore and approaches the active site. Although dispensable for Pol II binding, domain III is ordered in the electron density due to many contacts with Pol II (Figures 2A and 3B). The base of domain III forms a hydrophobic contact with Rpb1 residues 755-756 (Figure 3B). Several salt bridges can be formed between charged residues at the base of domain III and in helix  $\alpha 21$  and loop  $\beta 20$ - $\beta 21$  of Rpb1 (Figure

3B). The  $\beta$ -hairpin of domain III is highly flexible in free TFIIS (Qian et al., 1993), but is fixed here by contacts with polymerase regions that line the pore, including Rpb1 residues in the bridge (823-830) and trigger loop (1078-1080), and several Rpb2 residues (Figures 2A and 3B). The high conservation of the pore-lining regions befits the high conservation of TFIIS domain III (62% identical residues between yeast and human, Figure 2D).

### The TFIIS Acidic Hairpin Complements the Polymerase Active Site

TFIIS domain III reaches the Pol II active site with the highly conserved loop of the protruding  $\beta$ -hairpin (Figures 2B-2D). Two invariant acidic residues in this loop, D290 and E291, are in close proximity of the Pol II catalytic metal ion A. The two acidic hairpin residues are essential for TFIIS activity, and even conservative mutations of these residues render TFIIS inactive (Jeon et al., 1994). The domain III hairpin thus complements the polymerase active site with acidic groups that are essential for TFIIS function. Pol II apparently contains a single tunable active site for both RNA polymerization and cleavage, instead of two catalytic sites with distinct locations. It had been suggested previously that the active sites for RNA polymerization and cleavage are close together or even identical (Powell et al., 1996; Rudd et al., 1994; Wang and Hawley, 1993).

### RNA Cleavage

The approximate location of the TFIIS hairpin loop with respect to substrate RNA is revealed by superposition of our model with the previous Pol II elongation complex structure (Figure 4). The superposition shows that TFIIS

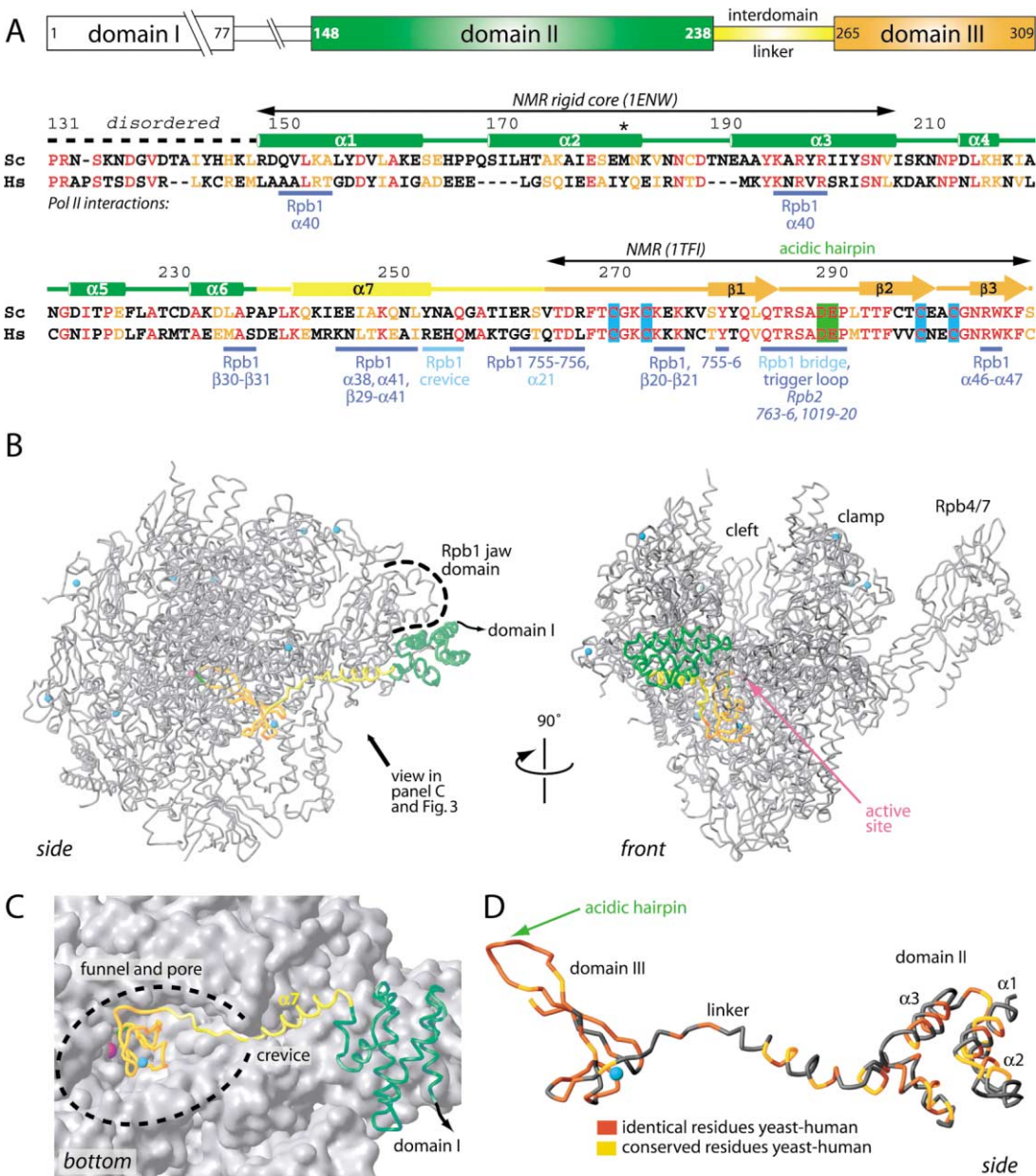


Figure 2. Architecture of the Pol II-TFIIIS Complex

(A) Domain organization and secondary structure of TFIIIS. The diagram shows TFIIIS domains with redefined borders. Secondary structure elements (cylinders,  $\alpha$  helices; arrows,  $\beta$  strands) are indicated above an alignment of TFIIIS sequences from the yeast *Saccharomyces cerevisiae* (Sc) and human (Hs). Identical and conserved residues are printed in red and light orange, respectively. The color code for TFIIIS domains is the same as described in the legend to Figure 1. Black double-headed arrows span regions for which available NMR structures (PDB accession codes in parentheses) were placed in the experimental electron density map. Residue M182 in domain II, which was located in the anomalous Fourier shown in Figure 1B, is indicated with an asterisk. The four cysteine residues that coordinate the zinc ion in domain III are highlighted in cyan, and the acidic hairpin residues D290 and E291 in light green. Regions in TFIIIS that are involved in Pol II interactions are underlined with blue bars. TFIIIS-interacting structural elements in Pol II subunits Rpb1 and Rpb2 are indicated below the blue bars. We refer to the nomenclature of Pol II domains and secondary structure elements introduced previously (Figures 2 and 3 in Cramer et al., 2001).

(B) Ribbon diagram of the Pol II-TFIIIS complex backbone model. The 12 subunits of Pol II are in silver. A pink sphere marks the location of the active site metal ion A (Cramer et al., 2000, 2001). Eight structural zinc ions in Pol II and one zinc ion in TFIIIS are depicted as cyan spheres. The two views are related by a 90° rotation around a vertical axis. The side view is as in Gnatt et al. (2001), and the front view is as in Armache et al. (2003) and Cramer et al. (2000, 2001).

(C) Binding of TFIIIS to the jaw, crevice, funnel and pore. TFIIIS is shown as a ribbon model on the molecular surface of Pol II. The view is from the bottom face, as indicated in (B).

(D) Conservation of TFIIIS. The view is from the side as in (B). Residues that are identical or conserved between yeast and human TFIIIS are in red and orange, respectively.

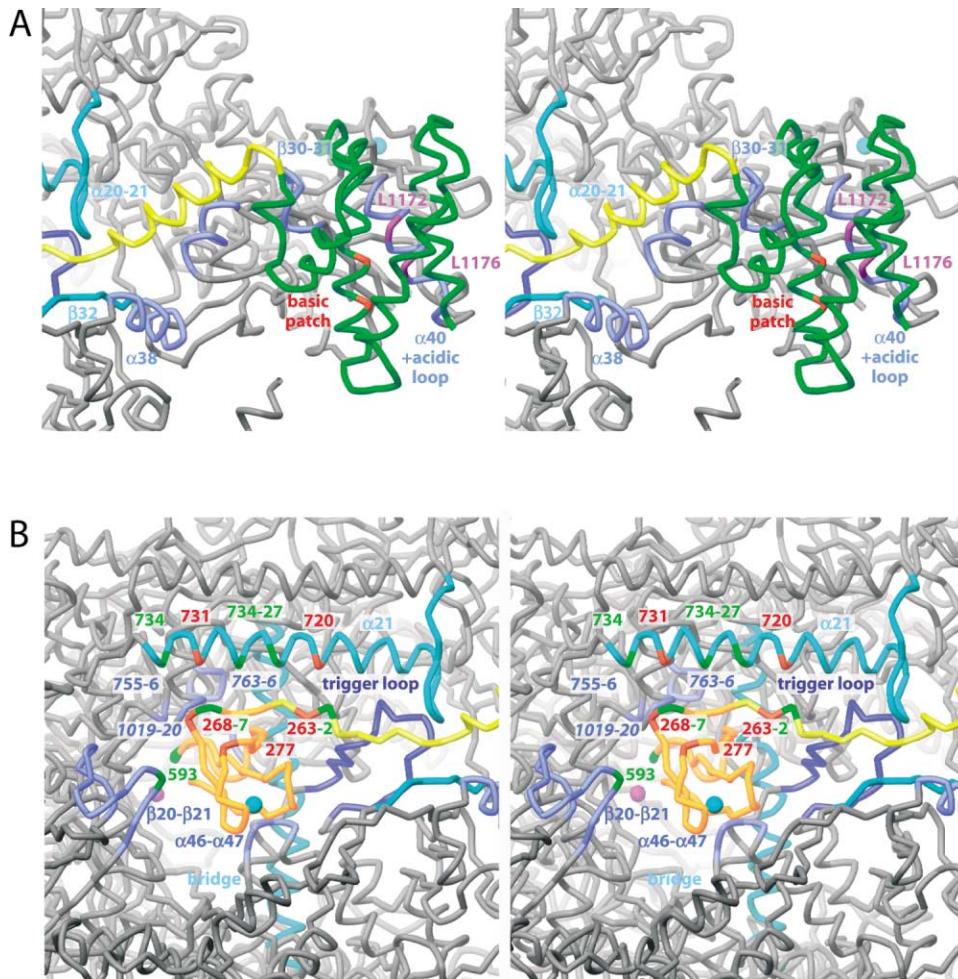


Figure 3. Details of Polymerase-TFIIS Interaction

(A, B) Two overlapping stereo views of a part of the model shown in Figure 2C, with the Pol II surface removed. Regions of Pol II that interact with TFIIS are labeled with plain and italic lettering for subunits Rpb1 and Rpb2, respectively.

domain III comes in close proximity of the RNA, consistent with crosslinking of the RNA 3' end to TFIIS (Powell et al., 1996). The two acidic residues in the TFIIS hairpin approach the sugar-phosphate backbone of the RNA, as required for catalytic RNA cleavage. The RNA phosphodiester bond that is potentially cleaved is observed in the elongation complex structure, since this complex is apparently trapped after nucleotide incorporation, but before translocation, adopting the pretranslocation state (Gnatt et al., 2001). The potential scissile phosphodiester bond (blue in Figure 4C) connects the 3'-oxygen in the ribose of the penultimate nucleotide with the  $\alpha$ -phosphorous of the terminal RNA nucleotide, since RNA cleavage leaves a 3'-OH group on the RNA, while liberating 5'-phosphonucleotides (Izban and Luse, 1993b).

The exact location of chemical groups in the active site cannot be determined at the resolution of our data. However, the location of the TFIIS hairpin and metal ion A with respect to the potential scissile RNA bond in the model suggests that the mechanism of RNA cleavage could resemble that of DNA cleavage by the Klenow DNA polymerase. In the Klenow exonuclease active site,

two catalytic metal ions are coordinated by acidic residues (Beese and Steitz, 1991; Joyce and Steitz, 1994). A first metal ion binds the 3' oxygen of the leaving ribose. A second metal ion and one of the acidic residues position a water molecule for an  $S_N2$ -type nucleophilic attack of the phosphorous atom from the side opposite the 3' oxygen, in-line with the scissile phosphodiester bond. In Pol II, metal A binds to the 3'-oxygen of the potential scissile bond. One of the TFIIS acidic hairpin residues could bind a metal ion B nearby, and could help position a water molecule for hydrolytic RNA cleavage. Such a mechanism would be consistent with the requirement for divalent metal ions in RNA cleavage by the Pol II-TFIIS complex (Izban and Luse, 1992; Reines, 1992; Wang and Hawley, 1993; Weilbaecher et al., 2003), and with evidence for a nucleophilic water molecule, coming from the observation of a dramatic increase in cleavage activity at high pH (Weilbaecher et al., 2003).

#### Switching between Polymerization and Cleavage

A two-metal-ion mechanism could thus underlie both RNA cleavage (see above) and RNA polymerization by Pol II (Cramer et al., 2001). Both polymerization and

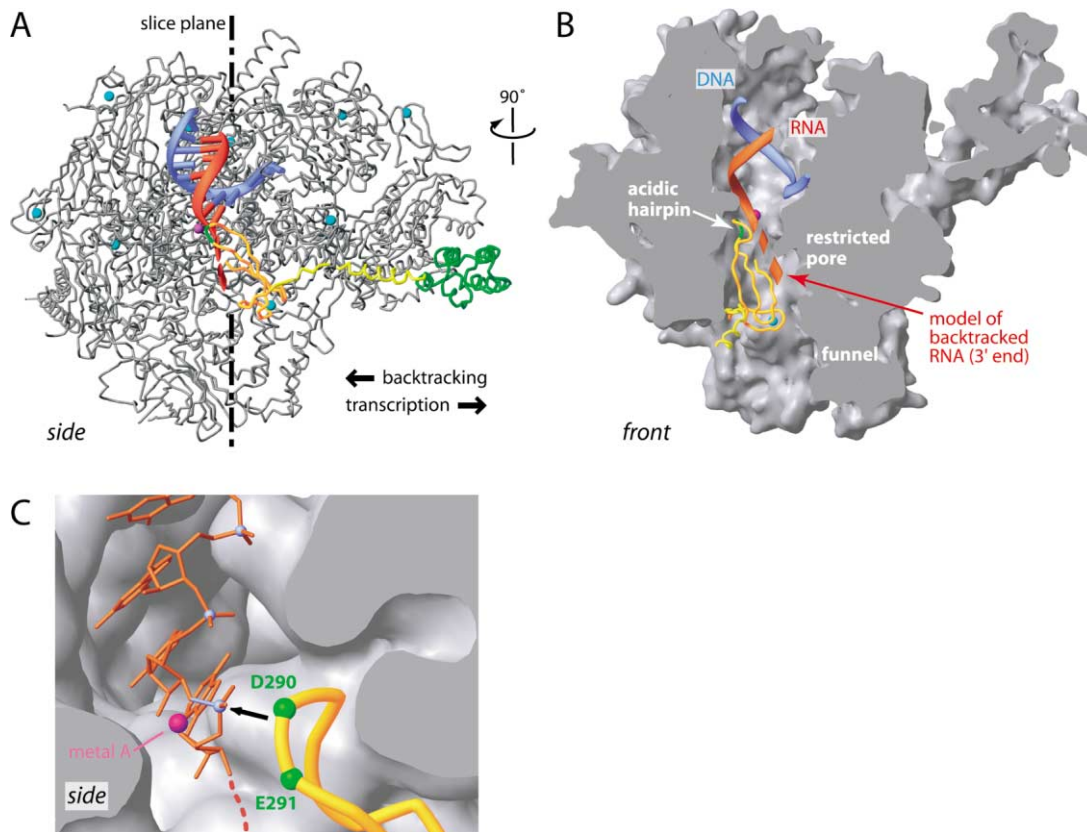


Figure 4. Model of a Pol II-TFIIS-Nucleic Acid Complex

(A) Side view. The DNA template strand (blue) and the RNA transcript (red) were placed onto the model of Figure 2B according to their location in the elongation complex structure (Gnatt et al., 2001). The Rpb2 protrusion, fork, and external domains were omitted for clarity. The presumed location of backtracked RNA is indicated as a dashed red ribbon. The arrows indicate movement of Pol II relative to the nucleic acids.

(B) Cut-away view of the model in (A) from the front. TFIIS and nucleic acids are shown as ribbon models on the molecular surface of Pol II, which is cut along the vertical slice plane indicated in (A). The presumed path of backtracked RNA through the restricted pore is drawn as a dashed red ribbon. The backtracked portion of RNA would be cut at the active site during TFIIS-induced RNA cleavage.

(C) Proximity of the TFIIS acidic hairpin to the potential scissile RNA phosphodiester bond. The view is as in (A). RNA was placed according to the location in the Pol II elongation complex structure (Gnatt et al., 2001), and is shown as a stick model with phosphorous atoms highlighted as blue spheres. The black arrow indicates the direction of a possible  $S_N2$ -type nucleophilic in-line attack of the scissile bond (blue).

cleavage apparently require a metal A that is persistently bound by the Rpb1 aspartate loop. Switching from polymerization to cleavage may however involve differential positioning of a mobile metal ion B. For polymerization, metal B could be recruited by the substrate nucleoside triphosphate (NTP, Cramer et al., 2001). For cleavage in the presence of TFIIS, the TFIIS acidic hairpin could contribute to metal B coordination. Cleavage in the absence of TFIIS, however, would likely require additional coordination partners for metal B. With a very recent analysis of the nuclease activity of bacterial RNA polymerase, Goldberg and coworkers provided evidence that during RNA cleavage metal B could be coordinated by the phosphates of an unpaired nucleotide bound to a site in the pore (Sosunov et al., 2003). Goldberg and coworkers further suggest a unified two-metal-ion mechanism for RNA synthesis and cleavage that is generally consistent with implications of our Pol II-TFIIS model. Whereas it was observed before that complementation of an enzyme active site with a residue from an external factor can enhance a catalytic activity (Scheffzek et al., 1997), the unique feature of Pol II is

its capability to switch between two distinct catalytic activities at a single active site.

### Proofreading

The available Pol II structures and many biochemical observations are consistent with the following model for mRNA proofreading. Incorporation of the correct nucleotide drives rapid forward translocation (Nedialkov et al., 2003). If the incorrect nucleotide is however incorporated, forward translocation is disfavored, opening a time window for hydrolytic RNA cleavage and removal of the misincorporated nucleotide. Alternatively, misincorporation can trigger backtracking by one nucleotide and subsequent cleavage of a dinucleotide. Cleavage of mononucleotides (from the pretranslocation state) and of dinucleotides (from a backtracked state) result in a new RNA 3' end at metal A, from which polymerization can continue. Proofreading may involve mainly cleavage of mono- and dinucleotides, so that extensive backtracking and RNA extrusion into the pore would not be required. Proofreading reactions can be stimulated by TFIIS *in vitro* (Jeon and Agarwal, 1996; Thomas et

al., 1998), but a contribution of TFIIS to proofreading *in vivo* may not be significant (Shaw et al., 2002).

#### Pore Restriction and RNA Backtracking

Our model shows that TFIIS domain III does not block the pore, but restricts it (Figure 4B). The restricted pore leaves enough space for NTP entry, as required for RNA polymerization in the presence of TFIIS (Horikoshi et al., 1984). Restriction of the pore may explain why TFIIS preferably releases dinucleotides (Izban and Luse, 1992, 1993a, 1993b). Modeling shows that RNA backtracking by more than one nucleotide would result in a clash with the TFIIS hairpin, unless RNA base stacking is given up, and the RNA is redirected and threaded into the restricted pore. The restricted pore is wide enough to accommodate an RNA single strand, and likely corresponds to an RNA binding site defined previously in Pol II-RNA binary complexes that undergo TFIIS-induced cleavage (Johnson and Chamberlin, 1994). Extensively backtracked RNA and TFIIS can thus bind simultaneously to the Pol II pore, as required for rescue of arrested Pol II complexes. Consistently, the backtracked RNA 3' end in an arrested bacterial RNA polymerase complex was crosslinked to a protein fragment that lines the restricted pore (Markovtsov et al., 1996).

#### TFIIS Remodels the Polymerase Active Center

In addition to a complementation of the Pol II active site, TFIIS induces structural changes in the active center (Figure 5A). These changes are revealed by a comparison of the Pol II-TFIIS complex with our recent model of the free 12-subunit Pol II (Armache et al., 2003). Since both models were obtained from the same crystal form, and since TFIIS binding does not induce significant changes in crystal packing or unit cell dimensions, the detected structural changes can be attributed to TFIIS binding.

Binding of TFIIS domain III induces folding of Rpb1 residues 1082–1091 (Figures 1C, 3B, and 5A), which correspond to the “trigger loop” in bacterial RNA polymerase (Vassilyev et al., 2002). TFIIS makes potential contacts to residues 1078–1080 just before the trigger loop. The folded trigger loop seals off a previously observed second perforation in the polymerase cleft (“pore 2,” Cramer et al., 2000). Structural changes in the trigger loop, and in the preceding helix  $\alpha$ 36, are propagated to the bridge helix (Figure 5A). TFIIS can form several potential contacts to Rpb1 residues 820–830, resulting in a movement of the C-terminal half of the bridge helix toward the top face of Pol II by 2–3 Å (Figures 1C and 5A). Changes in the bridge helix are further propagated to switch regions 1 and 2, which move slightly outward, resulting in a widening of the DNA-RNA hybrid binding site (Figure 5A), which may influence the strength of hybrid-polymerase interaction. Since both switches and the C-terminal half of the bridge helix interact with the DNA template strand in the elongation complex (Gnatt et al., 2001), changes in their position will reposition nucleic acids in the active center, maybe to facilitate RNA cleavage. Structural changes further include ordering of “fork loop 2” (Rpb2 residues 503–508, Figure 5A), which restricts the cleft to a diameter of 15 Å, consistent with the proposal that this loop removes the DNA non-

template strand from the template strand before the active site (Cramer et al., 2001; Gnatt et al., 2001).

#### Functional Conformations of Pol II

In addition to a local remodeling of the active center, TFIIS induces a coordinated repositioning of about one third of the polymerase mass (Figures 5C–5D). The repositioned mass includes the jaws, the clamp, and the Rpb1 cleft and foot domains, and corresponds essentially to three previously identified mobile polymerase modules (Cramer et al., 2001, Figure 5E). The mobile mass is tilted toward the top face of Pol II, by up to 6 Å at the jaws. The repositioning seems to be caused by insertion of TFIIS into the Pol II funnel and pore. In particular, the TFIIS linker opens the crevice, and TFIIS domain III forms a wedge between helix  $\alpha$ 21 and loop  $\alpha$ 46– $\alpha$ 47 in the Rpb1 funnel and cleft domains, respectively (arrows in Figure 5B). The mobile polymerase mass is connected to the remainder of the enzyme by the bridge helix, the switches, and the linker between the two Rpb9 domains, which all undergo structural changes to accommodate the repositioning.

A major conformational change in the polymerase upon TFIIS binding was suggested by functional studies of TFIIS and Pol II mutants (Cipres-Palacin and Kane, 1994; Hemming et al., 2000). There is also evidence for a conformational isomerization of Pol II upon the transition from initiation to elongation, and for distinct conformational states of elongating Pol II (Erie, 2002; Palangat and Landick, 2001). Since the mobile Pol II mass surrounds nucleic acids (Figure 5D), its repositioning could influence Pol II elongation properties, and the observed Pol II conformation may correspond to one of the functional states of the enzyme. Consistently, deletion of a region in bacterial RNA polymerase that corresponds to the Rpb1/9 jaw (Figure 5E) affects transcriptional pausing (Ederth et al., 2002).

#### Conservation of Transcript Cleavage Factors

Eukaryotic Pol III is capable of RNA cleavage, and its C11 subunit and magnesium ions are required for this activity (Chedin et al., 1998). C11 consists of two zinc ribbon domains. The C-terminal zinc ribbon shows high sequence similarity to domain III of TFIIS and comprises the two acidic hairpin residues. Since mutation of these two residues is lethal to yeast (Chedin et al., 1998), the C-terminal domain of C11 may function like domain III of TFIIS, with a corresponding acidic hairpin playing an essential role. The N-terminal domain of C11 is related in sequence to the N-terminal domain of Rpb9, and may occupy the same position, since only few amino acid residues would be required to connect it to its C-terminal domain that would be located in the pore. This model may also apply to the archaeal transcript cleavage factor TFS, which shows sequence similarity to C11, and contains the acidic hairpin residues (Hausner et al., 2000).

Bacteria do not contain a TFIIS homolog, but several lines of evidence had suggested that the bacterial transcript cleavage factors GreA and GreB function essentially like TFIIS. First, the binding site for GreB on bacterial polymerase corresponds to the rim of the Pol II funnel where TFIIS binds (Korzheva et al., 2000, 1997). Second, the structure of GreA, although different from that of

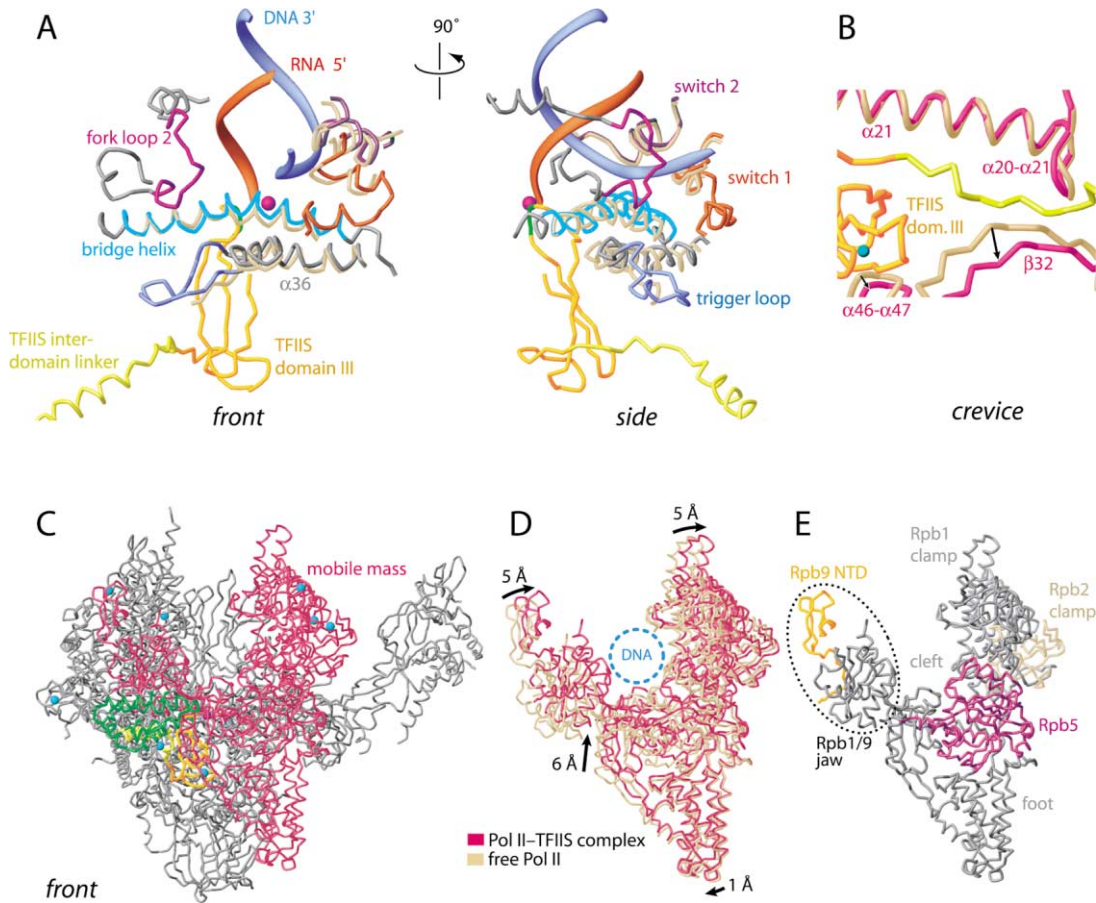


Figure 5. TFIS-Induced Structural Changes in Pol II

(A) Local remodeling of the Pol II active center. Structural elements of the active center in the Pol II-TFIS complex are shown as ribbons in different colors. The corresponding elements in the free 12-subunit Pol II structure are shown superimposed in beige. In the Pol II-TFIS complex, the trigger loop (blue) and fork loop 2 (pink) are folded, parts of the bridge helix (cyan) are shifted upward, and switches 1 and 2 (red and purple, respectively) moved outward. The DNA template strand (blue) and product RNA (red) have been placed according to the Pol II elongation complex structure (Gnatt et al., 2001). A pink sphere marks the location of metal ion A (Cramer et al., 2000, 2001). (B) Opening of the Pol II crevice and insertion of the TFIS linker. Detailed view of the TFIS linker (yellow) passing through the crevice (magenta). The location of the two crevice-forming elements in free Pol II is shown in beige. The view is from the bottom, as in Figures 2C and 3. (C–E) Global repositioning of the Pol II mobile mass. In (C), regions of the model in Figure 2B that are repositioned upon TFIS binding (mobile mass) are highlighted in magenta. In (D), changes in the mobile mass between free Pol II (beige) and the Pol II-TFIS complex (magenta) are shown. The models were superimposed based on the unchanged regions in the Pol II core module (Cramer et al., 2001). Arrows indicate the direction and magnitude of movements at outer positions. The location of the incoming DNA duplex during transcription elongation is indicated as a dashed blue circle. In (E), Pol II regions contributing to the mobile mass are shown. Subunits are colored according to the color code used previously (Armache et al., 2003; Cramer et al., 2000, 2001).

TFIS, shows a coiled-coil protrusion with acidic residues at the tip (Stebbins et al., 1995), which could reach the polymerase active site just like the TFIS acidic hairpin does. Third, like TFIS, Gre factors can be crosslinked to the RNA 3' end (Stebbins et al., 1995).

While this paper was in revision, a manuscript by Darst and coworkers became available that describes docking of structures of GreB and bacterial RNA polymerase to a 15 Å molecular envelope of the polymerase-GreB complex derived from electron microscopy (Opalka et al., 2003 [this issue of *Cell*]). Strikingly, these authors find that the coiled coil of GreB binds in the secondary channel of bacterial polymerase, which corresponds to the Pol II pore, and reaches the active site with its acidic tip. The authors further show that the acidic tip residues are critical for Gre factor function. These findings are

fully consistent with ours and demonstrate in a powerful way the conserved strategies employed for RNA cleavage stimulation by the structurally unrelated bacterial and eukaryotic RNA polymerase cleavage factors.

### Conclusions

We present here the X-ray structure analysis of a Pol II complex with a transcription factor. The Pol II-TFIS complex structure not only provides insights into the multiprotein interactions underlying factor function, it also helps understanding mRNA cleavage, proofreading, and conformational control of Pol II. Comparison with a corresponding bacterial complex (Opalka et al., 2003 [this issue of *Cell*]) highlights the conserved functional principles of transcript cleavage factors. Our anal-

ysis also supports the idea that DNA and RNA polymerases follow different strategies for nucleic acid cleavage and proofreading. In the Klenow DNA polymerase, the growing DNA shuttles between widely separated active sites for DNA synthesis and cleavage, whereas in Pol II the growing RNA remains at a single tunable active site that switches between RNA synthesis and cleavage modes.

#### Experimental Procedures

##### Cloning, Expression, and Purification of TFIIS

The gene encoding for a yeast TFIIS variant that includes domains II and III (residues 131–309) was amplified by PCR from *S. cerevisiae* genomic DNA, and subcloned into vector pET21b (Novagen). The TFIIS variant was expressed in *E. coli* as a fusion protein containing an amino-terminal hexahistidine tag, essentially as described (Awrey et al., 1997). Cells were lysed by sonication in buffer A (50 mM HEPES [pH 7.5], 300 mM NaCl, 5% glycerol, 0.3 mg/L leupeptin, 1.4 mg/L pepstatin A, 0.17 g/L PMSF, 0.33 g/L benzamidine, 10 mM  $\beta$ -mercaptoethanol, and 10  $\mu$ M ZnCl<sub>2</sub>). The lysate was cleared by centrifugation and was applied to a Ni-NTA agarose column (Qia-gen). The column was washed with buffer A containing 500 mM NaCl, and the protein was eluted with a gradient of 0 mM to 500 mM imidazole in buffer A containing 500 mM NaCl. Peak fractions were diluted 5-fold and loaded onto a Mono-S anion exchange column (Amersham) preequilibrated with buffer A containing 100 mM NaCl. The TFIIS variant was eluted over a total of 15 column volumes with a gradient of 100–500 mM NaCl in buffer A. This yields two peaks, which both contain the TFIIS variant, as confirmed by mass spectrometry. TFIIS in the two fractions shows the same apparent molecular weight in gel electrophoresis and gives rise to the same CD spectra. Fractions of the second peak were concentrated and applied to a Superose-12 gel filtration column (Amersham) equilibrated with buffer B (5 mM HEPES [pH 7.25], 40 mM ammonium sulfate, 10  $\mu$ M ZnCl<sub>2</sub>, 10 mM DTT). The TFIIS variant eluted as a monomer. Peak fractions were concentrated to 8 mg/mL, shock-frozen in liquid nitrogen, and stored at  $-80^{\circ}\text{C}$ . For selenomethionine incorporation, the TFIIS variant was introduced to the methionine auxotroph *E. coli* strain B834(DE3) (Budisa et al., 1995). Cells were grown in LB medium to an OD<sub>600</sub> of 0.7, were harvested, and were resuspended in selenomethionine-containing minimal medium (Budisa et al., 1995). Cells were grown for 60 min at  $20^{\circ}\text{C}$ , before expression was induced with 1 mM IPTG, and continued over night.

##### Crystallization and Multiprotein Complex Assembly

The yeast 10-subunit Pol II core and the Rpb4/Rpb7 heterodimer were purified as described, and the complete 12-subunit Pol II was reconstituted as described (Armache et al., 2003). Crystals were grown at  $20^{\circ}\text{C}$  with the sitting drop method by mixing 4  $\mu$ l of protein solution (4 mg/mL) with 2  $\mu$ l of reservoir solution (850 mM ammonium-sodium tartrate, 100 mM HEPES [pH 7.5], 5 mM DTT). Crystals grew to a maximum size of  $0.3 \times 0.15 \times 0.10$  mm. Crystals were transferred stepwise over a period of 8 hr to their mother solution containing additionally 0%–22% glycerol and 0–100 mM sodium ascorbate, before they were slowly cooled down to  $4$ – $8^{\circ}\text{C}$ , and incubated for another 24 hr. The solution was then exchanged by the same solution containing additionally 1 mg/mL of the purified TFIIS variant. Crystals were incubated for another 48–72 hr, mounted in cryo loops, and shock frozen by plunging into liquid nitrogen.

##### X-Ray Structural Analysis

Complete diffraction data to  $3.8 \text{ \AA}$  resolution were collected in two wedges of  $33^{\circ}$  and  $42^{\circ}$  with the use of phi-slicing with  $0.3^{\circ}$  increments at the protein crystallography beamline X06SA of the Swiss light source (Table 1). Higher resolution could not be obtained although many crystals and different cryocooling protocols were tested. Molecular replacement with AMORE (Navaza, 1994) resulted in a unique solution when the subunits Rpb1 and Rpb2 of the Pol II elongation complex structure (Gnatt et al., 2001) without the clamp were used as search model (Table 1). Using data in the range  $15$ – $7 \text{ \AA}$  resolution, the correlation coefficient for the correct solution was 44.1, com-

pared to 26.4 for the second best solution. Electron density maps were phased with the placed structure and were improved by solvent flipping. Pol II regions that had shifted upon TFIIS binding were omitted from map calculation and were manually docked to the resulting electron density map with the program O (Jones et al., 1991). After rigid body refinement with CNS (Brunger et al., 1998), the crystallographic R-factor was 39.2%, using all data in the range  $50$ – $3.8 \text{ \AA}$  resolution, and without adaptation of atomic positions or B-factors. The resulting electron density map allowed manual fitting of the rigid three-helical core of the NMR structure of yeast TFIIS domain II (Morin et al., 1996, Figure 1A), and the NMR structure of human TFIIS domain III (Qian et al., 1993). Strong peaks in anomalous Fourier maps calculated with native data and data from a crystal with selenomethionine-labeled TFIIS coincided with the location of the zinc ion in domain III and the side chain of Met182 in domain II, respectively, confirming the correct positioning of both TFIIS domains (Table 1, Figure 1B). Three additional helices in TFIIS domain II ( $\alpha 4$ – $\alpha 6$ ), the interdomain linker, and the  $\beta$ -hairpin loop in domain III were built into continuous electron density. Several newly ordered Pol II regions (Rpb1 trigger loop, Rpb1 acidic loop  $\alpha 40$ – $\beta 29$ , Rpb2 fork loop 2, Cramer et al., 2001) were also modeled as C $\alpha$ -backbones. An N-terminal  $\alpha$  helix of Rpb4 was extended by ten residues and the eight last ordered residues at the C terminus of Rpb1 were modeled as a helical fragment. At the resolution of the data, no refinement was carried out and the fitted structures were reduced to C $\alpha$  backbones.

#### Acknowledgments

We thank C. Schulze-Briese and the staff at beamline X06SA of the Swiss Light Source for help. We thank K.-P. Hopfner for help and discussions. We thank K. Strässer, R. Grosschedl, and members of the Cramer lab for comments on the manuscript. Supported by research grant CR117-2/1 of the Deutsche Forschungsgemeinschaft, by the EMBO Young Investigator Programme, and the Fonds der Chemischen Industrie.

Received: May 13, 2003

Revised: June 25, 2003

Accepted: July 3, 2003

Published: August 7, 2003

#### References

- Armache, K.-J., Kettenberger, H., and Cramer, P. (2003). Architecture of initiation-competent 12-subunit RNA polymerase II. *Proc Natl Acad Sci USA* *100*, 6964–6968.
- Awrey, D.E., Weilbaecher, R.G., Hemming, S.A., Orlicky, S.M., Kane, C.M., and Edwards, A.M. (1997). Transcription elongation through DNA arrest sites. A multistep process involving both RNA polymerase II subunit RPB9 and TFIIS. *J. Biol. Chem.* *272*, 14747–14754.
- Awrey, D.E., Shimasaki, N., Koth, C., Weilbaecher, R., Olmsted, V., Kazanis, S., Shan, X., Arellano, J., Arrowsmith, C.H., Kane, C.M., and Edwards, A.M. (1998). Yeast transcript elongation factor (TFIIS), structure and function. II: RNA polymerase binding, transcript cleavage, and read-through. *J. Biol. Chem.* *273*, 22595–22605.
- Beese, L.S., and Steitz, T.A. (1991). Structural basis for the 3'-5' exonuclease activity of Escherichia coli DNA polymerase I: a two metal ion mechanism. *EMBO J.* *10*, 25–33.
- Booth, V., Koth, C.M., Edwards, A.M., and Arrowsmith, C.H. (2000). Structure of a conserved domain common to the transcription factors TFIIS, elongin A, and CRSP70. *J. Biol. Chem.* *275*, 31266–31268.
- Brunger, A.T., Adams, P.D., Clore, G.M., DeLano, W.L., Gros, P., Grrosse-Kunstleve, R.W., Jiang, J.S., Kuszewski, J., Nilges, M., Pannu, N.S., et al. (1998). Crystallography & NMR system: A new software suite for macromolecular structure determination. *Acta Crystallogr D* *54*, 905–921.
- Budisa, N., Steipe, B., Demange, P., Eckerskorn, C., Kellermann, J., and Huber, R. (1995). High-level biosynthetic substitution of methionine in proteins by its analogs 2-aminohexanoic acid, selenomethionine, telluromethionine and ethionine in Escherichia coli. *Eur. J. Biochem.* *230*, 788–796.

- Bushnell, D.A., and Kornberg, R.D. (2003). Complete, 12-subunit RNA polymerase II at 4.1 Å resolution: implications for the initiation of transcription. *Proc. Natl. Acad. Sci. USA* *100*, 6969–6973.
- Bushnell, D.A., Cramer, P., and Kornberg, R.D. (2002). Structural basis of transcription:  $\alpha$ -amanitin-RNA polymerase II cocrystal at 2.8 Å resolution. *Proc. Natl. Acad. Sci. USA* *99*, 1218–1222.
- Carson, M. (1997). Ribbons. *Meth. Enzymol.* *277*, 493–505.
- Chedin, S., Riva, M., Schultz, P., Sentenac, A., and Carles, C. (1998). The RNA cleavage activity of RNA polymerase III is mediated by an essential TFIIIS-like subunit and is important for transcription termination. *Genes Dev.* *12*, 3857–3871.
- Cipres-Palacin, G., and Kane, C.M. (1994). Cleavage of the nascent transcript induced by TFIIIS is insufficient to promote read-through of intrinsic blocks to elongation by RNA polymerase II. *Proc. Natl. Acad. Sci. USA* *91*, 8087–8091.
- Cramer, P. (2002a). Multisubunit RNA polymerases. *Curr Opin Struct Biol* *12*, 89–97.
- Cramer, P. (2002b). Common structural features of nucleic acid polymerases. *Bioessays* *24*, 724–729.
- Cramer, P., Bushnell, D.A., Fu, J., Gnatt, A.L., Maier-Davis, B., Thompson, N.E., Burgess, R.R., Edwards, A.M., David, P.R., and Kornberg, R.D. (2000). Architecture of RNA polymerase II and implications for the transcription mechanism. *Science* *288*, 640–649.
- Cramer, P., Bushnell, D.A., and Kornberg, R.D. (2001). Structural basis of transcription: RNA polymerase II at 2.8 angstrom resolution. *Science* *292*, 1863–1876.
- Davie, J.K., and Kane, C.M. (2000). Genetic interactions between TFIIIS and the Swi-Snf chromatin-remodeling complex. *Mol. Cell Biol.* *20*, 5960–5973.
- Ederth, J., Artsimovitch, I., Isaksson, L.A., and Landick, R. (2002). The downstream DNA jaw of bacterial RNA polymerase facilitates both transcriptional initiation and pausing. *J. Biol. Chem.* *277*, 37456–37463.
- Erie, D.A. (2002). The many conformational states of RNA polymerase elongation complexes and their roles in the regulation of transcription. *Biochim. Biophys. Acta* *1577*, 224–239.
- Fish, R.N., and Kane, C.M. (2002). Promoting elongation with transcript cleavage stimulatory factors. *Biochim. Biophys. Acta* *1577*, 287–307.
- Gnatt, A.L., Cramer, P., Fu, J., Bushnell, D.A., and Kornberg, R.D. (2001). Structural basis of transcription: an RNA polymerase II elongation complex at 3.3 Å resolution. *Science* *292*, 1876–1882.
- Gu, W., and Reines, D. (1995). Variation in the size of nascent RNA cleavage products as a function of transcript length and elongation competence. *J. Biol. Chem.* *270*, 30441–30447.
- Hausner, W., Lange, U., and Musfeldt, M. (2000). Transcription factor S, a cleavage induction factor of the archaeal RNA polymerase. *J. Biol. Chem.* *275*, 12393–12399.
- Hemming, S.A., Jansma, D.B., Macgregor, P.F., Goryachev, A., Friesen, J.D., and Edwards, A.M. (2000). RNA polymerase II subunit rpb9 regulates transcription elongation in vivo. *J. Biol. Chem.* *275*, 35506–35511.
- Horikoshi, M., Sekimizu, K., and Natori, S. (1984). Analysis of the stimulatory factor of RNA polymerase II in the initiation and elongation complex. *J. Biol. Chem.* *259*, 608–611.
- Izban, M.G., and Luse, D.S. (1992). The RNA polymerase II ternary complex cleaves the nascent transcript in a 3'-5' direction in the presence of elongation factor SII. *Genes Dev.* *6*, 1342–1356.
- Izban, M.G., and Luse, D.S. (1993a). The increment of SII-facilitated transcript cleavage varies dramatically between elongation competent and incompetent RNA polymerase II ternary complexes. *J. Biol. Chem.* *268*, 12874–12885.
- Izban, M.G., and Luse, D.S. (1993b). SII-facilitated transcript cleavage in RNA polymerase II complexes stalled early after initiation occurs in primarily dinucleotide increments. *J. Biol. Chem.* *268*, 12864–12873.
- Jeon, C.-J., and Agarwal, K. (1996). Fidelity of RNA polymerase II transcription controlled by elongation factor TFIIIS. *Proc. Natl. Acad. Sci. USA* *93*, 13677–13682.
- Jeon, C., Yoon, H., and Agarwal, K. (1994). The transcription factor TFIIIS zinc ribbon dipeptide Asp-Glu is critical for stimulation of elongation and RNA cleavage by RNA polymerase II. *Proc. Natl. Acad. Sci. USA* *91*, 9106–9110.
- Johnson, T.L., and Chamberlin, M.J. (1994). Complexes of yeast RNA polymerase II and RNA are substrates for TFIIIS-induced RNA cleavage. *Cell* *77*, 217–224.
- Jones, T.A., Zou, J.Y., Cowan, S.W., and Kjeldgaard, M. (1991). Improved methods for building protein models in electron density maps and the location of errors in these models. *Acta Crystallogr.* *A47*, 110–119.
- Joyce, C.M., and Steitz, T.A. (1994). Function and structure relationships in DNA polymerases. *Annu. Rev. Biochem.* *63*, 777–822.
- Korzheva, N., Mustae, A., Kozlov, M., Malhotra, A., Nikiforov, V., Goldfarb, A., and Darst, S.A. (2000). A structural model of transcription elongation. *Science* *289*, 619–625.
- Koulich, D., Orlova, M., Malhotra, A., Sali, A., Darst, S.A., and Borukhov, S. (1997). Domain organization of *Escherichia coli* transcript cleavage factors GreA and GreB. *J. Biol. Chem.* *272*, 7201–7210.
- Markovtsov, V., Mustae, A., and Goldfarb, A. (1996). Protein-RNA interactions in the active center of transcription elongation complex. *Proc. Natl. Acad. Sci. USA* *93*, 3221–3226.
- Morin, P.E., Awrey, D.E., Edwards, A.M., and Arrowsmith, C.H. (1996). Elongation factor TFIIIS contains three structural domains: solution structure of domain II. *Proc. Natl. Acad. Sci. USA* *93*, 10604–10608.
- Navaza, J. (1994). AMoRe: an automated package for molecular replacement. *Acta Crystallogr.* *A50*, 157–163.
- Nedialkov, Y.A., Gong, X.Q., Hovde, S.L., Yamaguchi, Y., Handa, H., Geiger, J.H., Yan, H., and Burton, Z.F. (2003). NTP-driven translocation by human RNA polymerase II. *J. Biol. Chem.* *278*, 18303–18312.
- Nudler, E., Mustae, A., Lukhtanov, E., and Goldfarb, A. (1997). The RNA-DNA hybrid maintains the register of transcription by preventing backtracking of RNA polymerase. *Cell* *89*, 38–41.
- Olmsted, V.K., Awrey, D.E., Koth, C., Shan, X., Morin, P.E., Kazanis, S., Edwards, A.M., and Arrowsmith, C.H. (1998). Yeast transcription elongation factor TFIIIS, structure and function. I: NMR structural analysis of the minimal transcriptionally active region. *J. Biol. Chem.* *273*, 22589–22594.
- Opalka, N., Chlenov, M., Chacon, P., Rice, W.J., Wriggers, W., and Darst, S.A. (2003). Structure and function of the transcription elongation factor GreB bound to bacterial RNA polymerase. *Cell*, this issue, 335–345.
- Palangat, M., and Landick, R. (2001). Roles of RNA:DNA hybrid stability, RNA structure, and active site conformation in pausing by human RNA polymerase II. *J. Mol. Biol.* *311*, 265–282.
- Pokholok, D.K., Hannett, N.M., and Young, R.A. (2002). Exchange of RNA polymerase II initiation and elongation factors during gene expression in vivo. *Mol. Cell* *9*, 799–809.
- Powell, W., Bartholomew, B., and Reines, D. (1996). Elongation factor SII contacts the 3'-end of RNA in the RNA polymerase II elongation complex. *J. Biol. Chem.* *271*, 22301–22304.
- Qian, X., Gozani, S.N., Yoon, H., Jeon, C.J., Agarwal, K., and Weiss, M.A. (1993). Novel zinc finger motif in the basal transcriptional machinery: three-dimensional NMR studies of the nucleic acid binding domain of transcriptional elongation factor TFIIIS. *Biochemistry* *32*, 9944–9959.
- Reines, D. (1992). Elongation factor-dependent transcript shortening by template-engaged RNA polymerase II. *J. Biol. Chem.* *267*, 3795–3800.
- Rudd, M.D., and Luse, D.S. (1996). Amanitin greatly reduces the rate of transcription by RNA polymerase II ternary complexes but fails to inhibit some transcript cleavage modes. *J. Biol. Chem.* *271*, 21549–21558.
- Rudd, M.D., Izban, M.G., and Luse, D.S. (1994). The active site of RNA polymerase II participates in transcript cleavage within arrested ternary complexes. *Proc. Natl. Acad. Sci. USA* *91*, 8057–8061.
- Scheffzek, K., Ahmadian, M.R., Kabsch, W., Wiesmuller, L., Lautwein, A., Schmitz, F., and Wittinghofer, A. (1997). The Ras-RasGAP

complex: structural basis for GTPase activation and its loss in oncogenic Ras mutants. *Science* 277, 333–338.

Sekimizu, K., Kobayashi, N., Mizuno, D., and Natori, S. (1976). Purification of a factor from Ehrlich ascites tumor cells specifically stimulating RNA polymerase II. *Biochemistry* 15, 5064–5070.

Shaw, R.J., Bonawitz, N.D., and Reines, D. (2002). Use of an in vivo reporter assay to test for transcriptional and translational fidelity in yeast. *J. Biol. Chem.* 277, 24420–24426.

Shilatifard, A., Conaway, R.C., and Conaway, J.W. (2003). The RNA polymerase II elongation complex. *Annu. Rev. Biochem.* 72, 693–715.

Shimasaki, N.B., and Kane, C.M. (2000). Structural basis for the species-specific activity of TFIIS. *J. Biol. Chem.* 275, 36541–36549.

Sosunov, V., Sosunova, E., Mustaev, A., Bass, I., Nikiforov, V., and Goldfarb, A. (2003). Unified two-metal mechanism of RNA synthesis and degradation by RNA polymerase. *EMBO J.* 22, 2234–2244.

Stebbins, C.E., Borukhov, S., Orlova, M., Polyakov, A., Goldfarb, A., and Darst, S.A. (1995). Crystal structure of the GreA transcript cleavage factor from *Escherichia coli*. *Nature* 373, 636–640.

Thomas, M.J., Platas, A.A., and Hawley, D.K. (1998). Transcriptional fidelity and proofreading by RNA polymerase II. *Cell* 93, 627–637.

Vassilyev, D.G., Sekine, S., Laptenko, O., Lee, J., Vassilyeva, M.N., Borukhov, S., and Yokoyama, S. (2002). Crystal structure of a bacterial RNA polymerase holoenzyme at 2.6 Å resolution. *Nature* 417, 712–719.

Wang, D., and Hawley, D.K. (1993). Identification of a 3′-5′ exonuclease activity associated with human RNA polymerase II. *Proc. Natl. Acad. Sci. USA* 90, 843–847.

Weilbaecher, R.G., Awrey, D.E., Edwards, A.M., and Kane, C.M. (2003). Intrinsic transcript cleavage in yeast RNA polymerase II elongation complexes. *J. Biol. Chem.* 278, 24189–24199. Published online April 11, 2003.10.1074/jbc.M211197200.

Wind, M., and Reines, D. (2000). Transcription elongation factor SII. *Bioessays* 22, 327–336.

Woychik, N.A., and Hampsey, M. (2002). The RNA polymerase II machinery: structure illuminates function. *Cell* 108, 453–463.

Wu, J., Awrey, D.E., Edwards, A.M., Archambault, J., and Friesen, J.D. (1996). In vitro characterization of mutant yeast RNA polymerase II with reduced binding for elongation factor TFIIS. *Proc. Natl. Acad. Sci. USA* 93, 11552–11557.

#### Accession Numbers

The Protein Data Bank accession number for the Pol II-TFIIS complex model is 1PQV.